energies

MDPI

Article

Concentrated Solar Power with Thermoelectric Generator—An Approach Using the Cross-Entropy Optimization Method

João Ider *,†, Adhimar Oliveira †, Rero Rubinger †, Ana Karoline Silva †, Aluízio Assini †, Geraldo Tiago-Filho † and Marcia Baldissera †

Institute of Physics and Chemistry, Federal University of Itajuba, Av. BPS, 1303, Pinheirinho, Itajuba 37500-903, MG, Brazil; adhimarflavio@unifei.edu.br (A.O.); rero@unifei.edu.br (R.R.); anakaroline367@gmail.com (A.K.S.); aassini@hotmail.com (A.A.); gltiagofilho@gmail.com (G.T.-F.); mbaldissera@unifei.edu.br (M.B.)

* Correspondence: joaoiderfba@unifei.edu.br

† These authors contributed equally to this work.

Abstract: In this research, a Concentrated Solar Power (CSP) as a Parabolic Trough Collector (PTC), using Peltier cooling modules for power generation was analyzed by the Cross-Entropy method. When comparing conventional solar electric generators with this system, we have the advantage that it is compact and lightweight and can be easily assembled and used as low-cost power generation equipment. For this system, we perform I(V) measurements and use fit models to accurately extract the model parameters. This is all in a standalone, robust, and simultaneous fit of three equations, through the global optimization method called Cross-Entropy. This is a robust method that had never been applied to extract parameters in a thermoelectric generation.

Keywords: Concentrated Solar Power; Parabolic Trough Collector; Seebeck effect; Cross-Entropy; optimization method; efficiency

Citation: Ider, J.; Oliveira, A.; Rubinger, R.; Silva, A.K.; Assini, A.; Tiago-Filho, G.; Baldissera, M. Concentrated Solar Power with Thermoelectric Generator—An Approach Using the Cross-Entropy Optimization Method. *Energies* **2022**, *15*, 4774. https://doi.org/10.3390/en15134774

Academic Editors: Valerio Paolini, Francesco Gallucci and Andrea Aquino

Received: 13 May 2022
Accepted: 16 June 2022
Published: 29 June 2022

1. Introduction

The world is going through a transition. The energy sector is transforming to be more sustainable, safe, and economical in the future [1]. One of the pillars of this transition is renewable energy and is fueled by public stress and political action, spurred by the United Nations Sustainable Development Goals, increasing air pollution and water stress, as well as growing concerns about climate change. Innovation is a key factor, and the energy sector is evolving even further [2].

Rapid declines in renewable energy costs, particularly for solar and wind generation, have boosted the energy sector, which is leading the ongoing energy transition [3]. For example, between 2010 and 2018, prices fell sharply. Solar photovoltaic (PV) modules decreased by 90%. The cost of electricity of solar photovoltaic energy decreased by 77%. The per-unit price of wind turbines has halved over the same period, and the cost of electricity of onshore wind electricity has dropped by nearly 30%, with further dramatic drops expected over the next decade [4].

The energy sector transition and falling prices are accelerated by three main innovation trends: (1) digitalization, (2) decentralization, and (3) electrification. These trends are shifting paradigms, roles, and responsibilities, opening doors to new players in the industry, and freeing up system flexibility for a high share of Variable Renewable Energy (VRE) penetration. In this article, we propose to make a contribution to the construction of knowledge in the number one trend, digitization.

Digitization can be defined as the conversion of data into value for the power sector. For several decades, the use of digital technologies, whether monitoring or control, in the fields of energy generation and transmission has been a trend. Recently they have begun to penetrate even further into energy systems. The use of the Internet of Things, the more

general application of smart meters and sensors, and the use of a lot of data with artificial intelligence have created new opportunities, providing the system with new services [5,6].

There are several technologies used for the use of renewable energies, including PV, Wind, Biomass, and Concentrated Solar Power (CSP), which will be the subject of study here.

CSP is a viable form of power generation with many power plants and variable forms of power generation scattered throughout the world [7]. CSP technologies focus heat in one area to produce the high temperatures required to make electricity. Since the solar radiation that reaches the Earth is spread out and diluted, it must be concentrated to produce the high temperatures required to generate electricity. There are several types of technologies that use mirrors or other reflecting surfaces to concentrate the sun's energy up to 2000 times its normal intensity [8].

Parabolic Trough Collectors (PTC) use long reflecting troughs that focus the sunlight onto a pipe located at the focal line. The first parabolic-trough system was developed in 1912 in Cairo, Egypt [9]. A fluid circulating inside the pipe collects the energy and transfers it to a heat exchanger, which produces steam to drive a turbine. One of the world's largest parabolic trough power plants is located in the Mojave Desert in California. This collection of plants has a total generating capacity of 354 megawatts, one-third the size of a large nuclear power plant [10].

Global CSP capacity grew 11% in 2019 to 6.2 GW, with 600 MW of capacity coming online. This was down from the 700 MW commissioned in 2018 and well below the average annual increase (24%) of the past decade. However, CSP continued to spread to new markets, and more than 1.1 GW of additional capacity was under construction at year's end, as seen in the Figure 1.

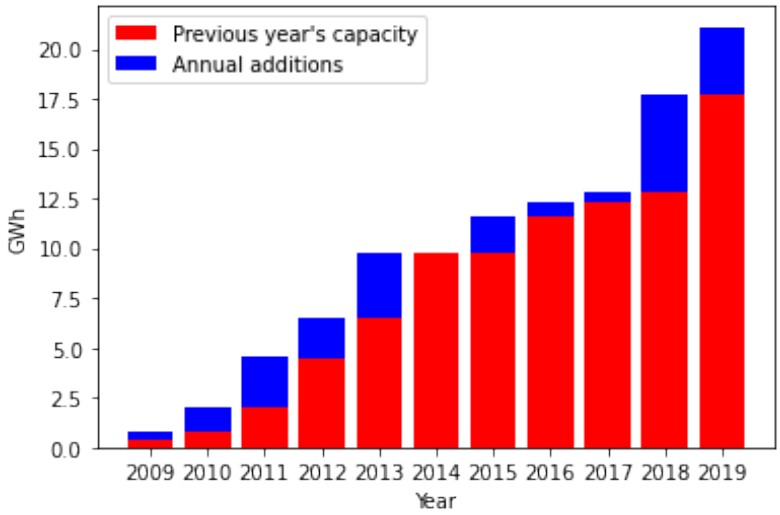

Figure 1. CSP Thermal Energy Storage Global Capacity and Annual Additions, 2009–2019 [11].

To deal with intermittency associated with PV [12] and wind power generation [13], limits of radiation absorption spectral range [14] and also efficiency decreases due to temperature effects on PV [15], the use of the Thermoelectric Generator (TEG) alone or in association with PV technology must be considered. One remarkable advantage of TEGs against PV is that it generates energy more effective under cloudy weather [16] since long wavelength radiation is less subject to being contained by clouds being an effective form to cope with PV intermittency.

TEG Technology is based on a single effect that is the Seebeck effect. Seebeck effect is caused by the diffusion of carriers from the hot to the cold side of the sample building a difference of potential between them [17,18].

With proper adaptations, CSP can be used with heat storage, allowing its use for power generation even at night or in cloudy environments. Also, according to Singh et al. [19],

the association of CSP with TEG technology is advantageous since it allows power generation without mechanical parts such as electrical generators, and capacitors among other components, being noiseless, reliable, and environment friendly. For this, TEGs convert heat energy from a temperature gradient that established a small voltage in the opposite terminals a pn junction of a thermoelectric material due to the Seebeck effect [20]. A TEG module is composed of more than a hundred such junctions.

To analyze TEG measurements, it is important to consider a proper theoretical background [21–25]. For a TEG device, power is derived from thermodynamics first law considering internal power dissipation RI^2 or as a function of load resistance, as shown in Equation (1).

$$P = NI[S(T_h - T_c) - RI] = NI^2R_L \tag{1}$$

where N stands for several pn junctions, S is the Seebeck coefficient, I the current through the TEG, R its internal resistance, T_h e T_c are the temperatures from the hot and cold sides respectively, and R_L is the load resistance.

Using an Equation (1) we get the voltage across the load resistance (Equation (2)) and the current (Equation (3)).

$$V = NI[S(T_h - T_c) - RI]. \tag{2}$$

$$I = \frac{S(T_h - T_c)}{R_L + R}. \tag{3}$$

Here, we can see that the current is not a function of the number of pn junctions.

Applying Equations (2) and (3), we can write the power in the form presented in Equation (4).

$$P = \frac{NS^2(T_h - T_c)^2}{R} \frac{R_L/R}{(1 + R_L/R)^2}. \tag{4}$$

Considering the heat equation, thermal efficiency is the ratio between the output power and the heat absorbed from the hot side

$$\eta = \frac{P}{\phi}, \tag{5}$$

where the power per modulus P is $P_{max}/8$ and the heat flux ϕ is

$$\phi = \frac{\kappa B \Delta T}{w}, \tag{6}$$

where w the thickness, B the surface area and κ is the thermal conductivity. The Equation (5) can be rewritten as

$$\eta = \frac{\left(1 - \frac{T_c}{T_h}\right)\frac{R_L}{R}}{\left(1 + \frac{R_L}{R}\right) - \frac{1}{2}\left(1 - \frac{T_c}{T_h}\right)\frac{\left(1 + \frac{R_L}{R}\right)^2 \frac{T_c}{T_h}}{ZT_c}}, \tag{7}$$

where $ZT_c = \frac{S^2 T_c}{\kappa\rho}$ and the ρ is electrical resistivity. It is also important to consider a comparison with the thermal efficiency of an ideal Carnot machine given by

$$\eta_c = 1 - \frac{T_c}{T_h}. \tag{8}$$

The maximum efficiency is obtained with $R_L = R$, so that

$$\eta_{max} = \left(1 - \frac{T_c}{T_h}\right) \frac{\sqrt{1 + Z\bar{T}} - 1}{\sqrt{1 + Z\bar{T}} + \frac{T_c}{T_h}}, \tag{9}$$

where $\bar{T}$ is the average temperature between the hot and cold junction temperatures and the maximum power equation is

$$P_{max} = \frac{NS^2(T_h - T_c)^2}{4R}. \tag{10}$$

Finally, the effective resistivity is

$$\rho = \frac{4P_{max}A/L}{N(I_{max})^2}, \tag{11}$$

and the effective Z-factor is

$$Z_{eff} = \frac{1}{\bar{T}}\left[\left(\frac{1+\frac{T_c\eta_{max}}{T_h\eta_c}}{1-\frac{\eta_{max}}{\eta_c}}\right)^2 - 1\right]. \tag{12}$$

Thus, this work consists of the experimental measurements of I(V) characteristics of a parabolic solar concentrator with Peltier modules in its focus and its subsequent analysis by a Cross-Entropy optimization method considering here presented equations. In the following, we will describe our experimental setup and methods.

2. Materials and Methods

For this work, we analyzed a CSP whose patent was registered in [26]. An iron bar was designed and fixed to the sides of the CSP so that it is above, along the center of the parabolic axis. Eight TECs, Danvic brand, model HC-40-15.4, were placed at the bottom of the bar. These TECs had the hot side facing down, towards the center. The cold side was up, fixed to the iron bar. Inside the iron bar, there is a stream of water, which comes directly from the side. This flow of water inside the iron bar causes the side of the TEC that is in contact with it to stay cool as well. This schematic is shown in Figure 2 and the real image shown in Figure 3.

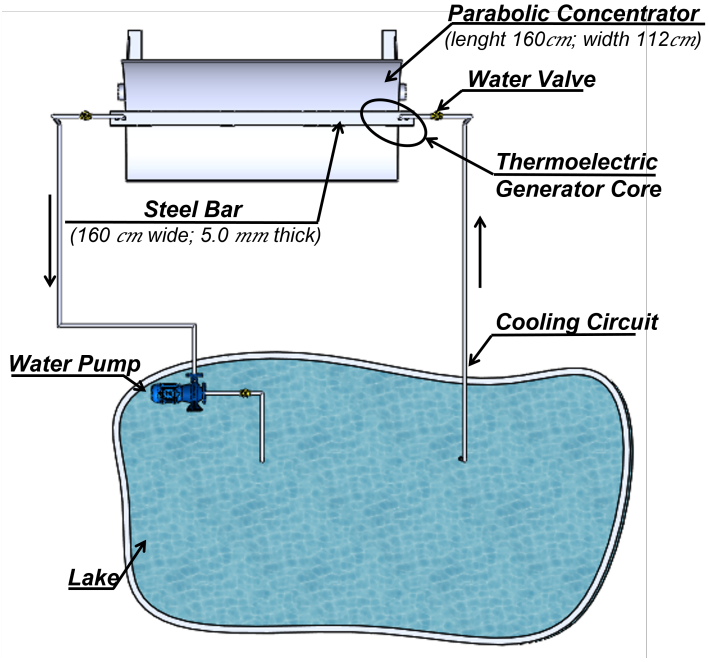

Figure 2. Schematics of the generator setup of the cylindrical-parabolic collector with dimensions. Main parts are indicated on the Figure.

Figure 3. Concentrated Solar Power as a Parabolic Trough Collector.

The lake used for this experiment is large, and has a large mass of water, so its temperature remains constant. Two type-K thermocouples were used to measure temperatures. One of them measured the temperature of the cold side, the contact between the iron bar and the TEC, called T_c, and the other measured the hot temperature, the side of the TEC that was facing the center of the CSP, called T_h, the side that will receive the sun's rays concentrated by the reflecting parabola.

A portable Reed Instruments DW-6060 watt meter was used to measure electrical output power. With it we were able to measure voltage, current, and power and a precision potentiometer of 100 kΩ. As the measurements were carried out far from the laboratory, these instruments were the most indicated because of the battery. Current-voltage data were collected with a constant temperature gradient along with each measurement. The measured current I and voltage V give us directly the power P and the load resistance R_L calculated according to Equation (2).

3. The Cross-Entropy Optimization Method

The Cross-Entropy (CE) method is an interactive optimization method that applies to continuous and discrete problems. It minimizes the entropy between the distribution of solutions in the objective function, choosing the best sample for the next interaction. The CE was introduced by Rubinstein [27] to estimate the probability of rare events in stochastic and discrete optimization networks. The CE has been applied to several optimization problems, such as alignment of DNA sequences [28], adjustments of isochrones in open clusters [29,30], thickness estimation in thin films [31] and electronic mobility in semiconductors [32], showing a robust method for the solution of parameter estimation. The CE uses sampling concepts, being a technique of reduction of variance, but that does not require a priori knowledge of the parameters regarding distribution. The CE consists of a simple adaptive procedure for estimating parameters. Furthermore, the CE procedure is based on a solution space, with an evolutionary rule in which a fraction of the space is selected in each iteration based on some selection criteria.

Each CE method interaction follows these steps:

1. Initial sample generation of the set of parameters to be estimated through normal distributions, following the rule

$$v_n^j = N(\mu^j, \sigma^j, n), \tag{13}$$

where N is a normal distribution centered between the pre-specified physical intervals μ^j, n is the number of entities of the distribution, which in this research were adopted 100 entities, j is the number of parameters to be adjusted, which here is equal to 4 and

σ^j is the variation of the distribution of solutions that are initially adopted between the pre-specified lower and upper physical limits;

2. Select 10% of the best solutions, v^j_{best} based on the negative logarithm of likelihood. For this, a comparison occurs through an objective function between the experimental data of power, current, and voltage, with the models obtained through the Equations (2)–(4);
3. Random generation of a new distribution of parameters using the values of v^j_{best} to generate the center of the distribution, μ and for the variation of the distribution, σ, following the rule:

$$\mu^j = \alpha\mu(v^j_{best}) + (1-\alpha)\mu(v^j_{best}), \tag{14}$$

$$\sigma^j = \alpha\sigma(v^j_{best}) + (1-\alpha)\sigma(v^j_{best}), \tag{15}$$

where $\mu(v^j_{best})$ is the mean value of the distribution v^j_{best} for each parameter j and $\sigma(v^j_{best})$ the standard deviation. The α parameter determines the convergence speed for the solution and doesn't allow the method to get stuck in a local minimum;
4. The method returns to the first for until a pre-specified criterion is satisfied.

In this work, we opted for a random resampling of the data. For that, we used the Bootstrap [33] technique, which is a repetition technique in which some experimental data are removed and randomly added to make the procedure in which it was inserted more robust. In this work, the data were resampled 50 times, producing good statistics on the parameters found.

4. Discussion

The equipment was tuned up and tested for its ability to reach high temperatures and we chose a rolled-up day for the experiment. Several measurements of I(V) curves were performed and for our analyses, we highlight six of them. The measurements are shown in the Table 1 along with the temperature gradients, which are between 52 °C and 109 °C.

Table 1. Measurement list with hot, cold and temperature gradients together with measured sun radiation power.

Measurement	T_h (°C)	T_c (°)	ΔT (°C)	Sun Radiation (Wm^{-2})
1	90	38	52	640
2	95	38	57	680
3	108	38	70	693
4	118	37	81	753
5	128	38	90	865
6	138	29	109	966

The experimental data with the respective fittings of our experiment are shown in Figure 4. Measured values are represented by dots and fittings by lines.

The data collected in the field were limited to a small voltage range and showed some fluctuations. They were treated under the Cross-Entropy optimization method. These measurements are difficult to perform and the same temperature cannot be guaranteed at all points on the device's surface, so the data appear non-linear for higher temperature gradients, however, it is just a thermodynamic effect due to variation.

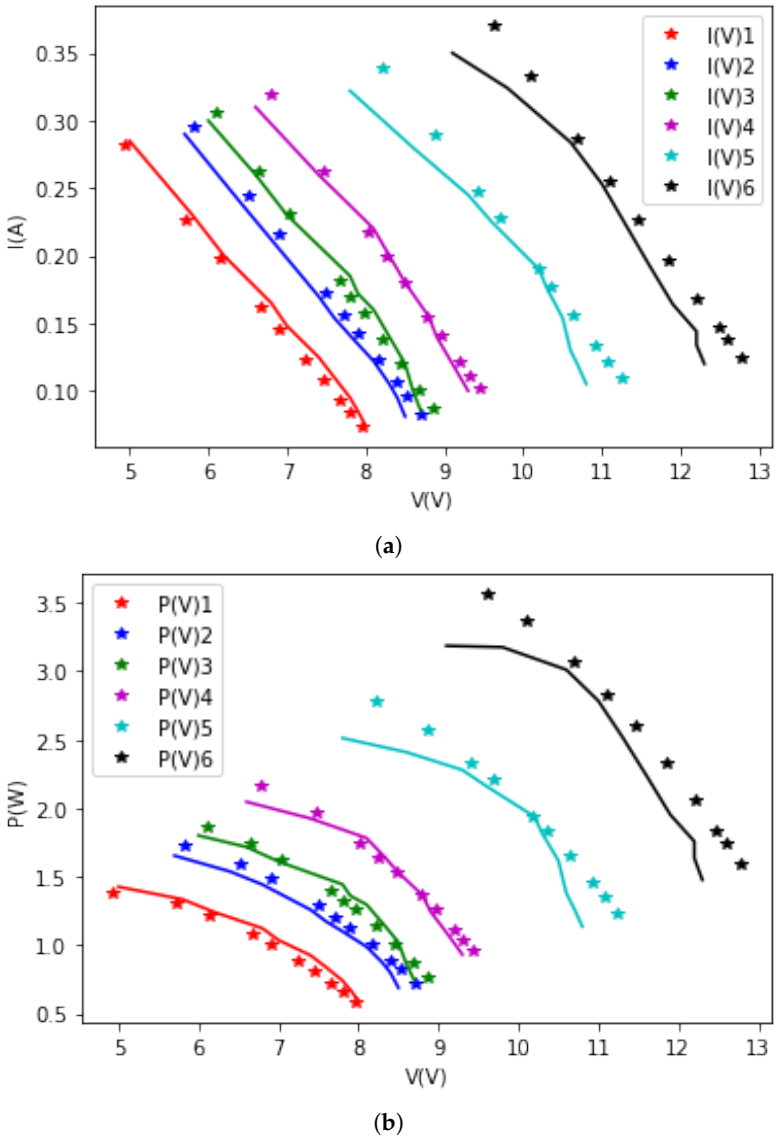

Figure 4. Experimental data for I(V) characteristics (dots) and power P(V) (dots) and fitted data (lines of same colors) for the collector system. Data corresponds to Table 1 in the order: (**a**) I(V) measurements 1 to 6, (**b**) P(V) measurements 1 to 6.

Parameter fitting errors were kept within acceptable limits, as can be seen in Table 2. The ratio V/(NI), Equation (2), determines the value of R_L and with that, we make the simultaneous fitting of I(V) and P(V), because, for this, we consider I(R_L), V(R_L).

Table 2. Search Space Results. The four first parameters from left are fitting results and the two others measures fitting quality. S, R here are considered as the mean value for a single pn junction unit inside a module.

	S (mVK^{-1})	**R (Ω)**	**T$_h$ (°C)**	**T$_c$ (°C)**
1	0.17	0.0143 ± 0.0003	90.0 ± 0.3	37.5 ± 0.2
2	0.17	0.0134 ± 0.0003	94.9 ± 0.4	38.1 ± 0.4
3	0.14	0.0124 ± 0.0009	107.9 ± 0.3	38.1 ± 0.3
4	0.13	0.0117 ± 0.0009	117.9 ± 0.3	37.1 ± 0.3
5	0.14	0.0126 ± 0.0016	128.0 ± 0.3	38.1 ± 0.3
6	0.13	0.0128 ± 0.0011	137.9 ± 0.2	29.1 ± 0.2

From the graphs, it can be seen that I(V) is almost linear and P(V) is parabolic. If we look at the Equation (1) until the Equation (4), we will notice that the variables are interdependent, therefore, difficult to be isolated. The Cross-Entropy method, applied here, worked with excellent convergence for S, R.

In the Table 3 we present relevant parameters to analyze the performance of the CSP. In them we have short-circuit current I_{sc}, open-circuit voltage V_{oc}, maximum power point P_{max}, voltage at maximum power point $V(P_{max})$, and current at maximum power point $I(P_{max})$.

The thermoelectric performance is presented by Z_{eff}, the effective Figure of Merit, and the electrical resistivity by ρ.

The last two parameters are related to CSP efficiency. One is the theoretical limit η_c of the efficiency of a perfect Carnot engine and the other η_{max} the efficiency of the CSP at the maximum power point.

If we compare the performance of commercial PV, the CSP power generation results are low, however, two things need to be remembered. First, CSP is a technology in its early stages of development, when compared to PV technology. Second, it captures most of the energy in a region of the electromagnetic spectrum where PV technology does not absorb energy.

Table 3. Calculated parameters from the fitting data and model.

	I_{sc} (A)	V_{oc} (V)	P_{max} (W)	$V(P_{max})$	$I(P_{max})$	Z_{eff} (K^{-1})	ρ ($m\Omega$)m	η_c (%)	η_{max} (%)
1	0.63 ± 0.01	9.06 ± 0.07	1.38849	4.93554	0.28133	0.0026	2.52 ± 0.10	58.3 ± 0.3	3.11 ± 0.02
2	0.72 ± 0.02	9.78 ± 0.16	1.72117	5.81634	0.29592	0.0026	2.37 ± 0.14	59.9 ± 0.4	3.35 ± 0.03
3	0.79 ± 0.06	9.95 ± 0.18	1.86300	6.10410	0.30521	0.0026	2.13 ± 0.32	64.7 ± 0.3	4.07 ± 0.02
4	0.89 ± 0.07	10.65 ± 0.13	2.16587	6.79059	0.31895	0.0026	1.92 ± 0.29	68.5 ± 0.3	4.67 ± 0.03
5	0.98 ± 0.13	12.50 ± 0.50	2.78694	8.21642	0.33919	0.0026	2.10 ± 0.60	70.2 ± 0.2	5.14 ± 0.02
6	1.09 ± 0.10	14.20 ± 0.40	3.55976	9.62048	0.37002	0.0026	2.10 ± 0.40	78.9 ± 0.2	6.20 ± 0.02

η_{max} is a calculated theoretical value, being a maximum allowed thermodynamic limit. To calculate the value of the real efficiency, we use the Equations (5) and (6) with w = 0.00324 m, B = 0.0016 m^2 and κ = 1.5 $Wm^{-1}K^{-1}$. The result of the power generated by each module and the efficiency is presented in Table 4.

Table 4. Value of power generated by each module and actual efficiency.

	P (W)	η (%)
1	0.1736	0.45
2	0.2151	0.51
3	0.2329	0.45
4	0.2707	0.45
5	0.3484	0.52
6	0.4450	0.55

These results show us a good behavior of the Concentrated Solar Power with the use of thermoelectric generators and, mainly, the robustness of the applied mathematical method, the Cross-Entropy, which obtained results consistent with those already presented in the literature, thus showing an excellent alternative for application in the energy sector, especially in this case for a thermoelectric generation.

In Figure 5 we present all the values of Tables 3 and 4 in graphical form. This facilitates the visualization and understanding of the results presented.

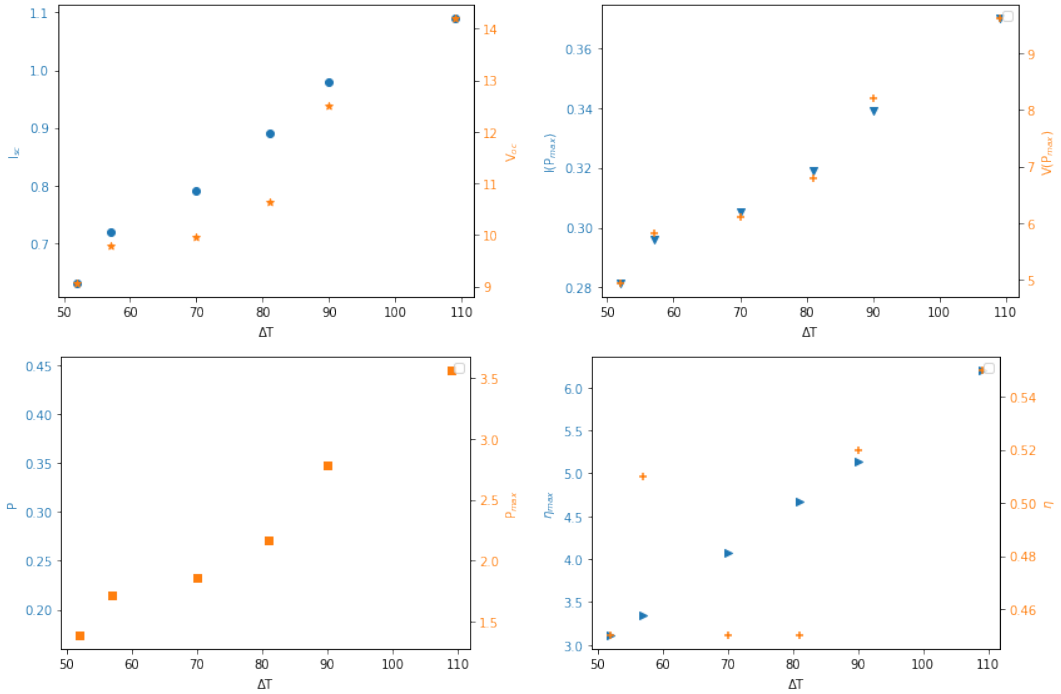

Figure 5. Values from the Tables 3 and 4.

In Table 5, comparing with another computational method applied to the same CSP model present in the literature in [34], we see a satisfactory behavior of the Cross-Entropy.

Table 5. Comparison of the values obtained by Cross-Entropy (η_{ce}) with values from the literature (η_{li}) in [34].

	η_{ce} (%)	η_{li} (%)
1	0.45	0.46
2	0.51	0.50
3	0.45	0.44
4	0.45	0.45
5	0.52	0.52
6	0.55	0.54

5. Conclusions

We have analyzed a Concentrated Solar Power for energy harvesting using Thermoelectric Generator technology based on eight Peltier cooler modules and parabolic mirrors with the Cross-Entropy optimization method. Voltage, current, and power (V, I, P) datapoints were subject to Cross-Entropy optimization method fittings simultaneous V, I, P as a function of the load resistance to obtain maximal consistency and accurate parameter extraction. Considering the best temperature gradient of 109 °C we obtained an efficiency of 6.20% as the thermodynamic limit for direct conversion from heat to electric power. This is an excellent result considering that thermoelectric generation technology by the use of semiconductor thermoelectric properties is still under development. The proposed mathematical optimization method, Cross-Entropy, for analysis proved to be very robust, presenting results consistent with those already presented in the literature, thus proving to be an excellent alternative for application in the energy sector, especially in this case for a thermoelectric generation.

The use of this simple construction and maintenance mechanism, using TECs and a metallic mirror, is promising for the generation of clean and environmentally sustainable energy. In addition, through the Cross-entropy optimization method, it is possible to find

the temperature range in which the system presents better performance, helping in the construction project of other systems of different dimensions.

Author Contributions: Conceptualization, J.I., A.O., R.R., A.A., G.T.-F. and M.B.; Data curation, J.I., A.O. and A.K.S.; Formal analysis, J.I., A.O. and G.T.-F.; Funding acquisition, A.A., G.T.-F. and M.B.; Investigation, R.R., A.K.S., A.A. and M.B.; Methodology, J.I., A.O., G.T.-F. and M.B.; Project administration, A.O. and R.R.; Resources, R.R., A.A., G.T.-F. and M.B.; Software, J.I., A.O. and A.K.S.; Supervision, G.T.-F.; Validation, J.I., A.O., R.R., G.T.-F. and M.B.; Visualization, J.I., A.A. and M.B.; Writing—original draft, J.I., A.O., A.K.S. and G.T.-F.; Writing—review & editing, J.I., A.O. and R.R. All authors have read and agreed to the published version of the manuscript.

Funding: This research was funded by Brazilian agencies CAPES, CNPq, and FAPEMIG.

Institutional Review Board Statement: Not applicable.

Informed Consent Statement: Not applicable.

Conflicts of Interest: The authors declare no conflict of interest.

References

1. Olabi, A.; Abdelkareem, M.A. Renewable energy and climate change. *Renew. Sustain. Energy Rev.* **2022**, *158*, 112111. [CrossRef]
2. IRENA. *Innovation Landscape for a Renewable-Powered Future: Solutions to Integrate Variable Renewables*; IRENA: Abu Dhabi, United Arab Emirates, 2019.
3. Luderer, G.; Madeddu, S.; Merfort, L.; Ueckerdt, F.; Pehl, M.; Pietzcker, R.; Rottoli, M.; Schreyer, F.; Bauer, N.; Baumstark, L.; et al. Impact of declining renewable energy costs on electrification in low-emission scenarios. *Nat. Energy* **2022**, *7*, 32–42. [CrossRef]
4. Irena, I. *Renewable Power Generation Costs in 2017*; Report; International Renewable Energy Agency: Abu Dhabi, United Arab Emirates, 2018.
5. Xu, Q.; Zhong, M.; Li, X. How does digitalization affect energy? International evidence. *Energy Econ.* **2022**, *107*, 105879. [CrossRef]
6. Bernabé-Moreno, J. When digitalization becomes an essential part of our energy transition. *Digit. Welt* **2022**, *6*, 8–13. [CrossRef]
7. Noč, L.; Jerman, I. Review of the spectrally selective (CSP) absorber coatings, suitable for use in SHIP. *Sol. Energy Mater. Sol. Cells* **2022**, *238*, 111625. [CrossRef]
8. Islam, M.T.; Huda, N.; Abdullah, A.; Saidur, R. A comprehensive review of state-of-the-art concentrating solar power (CSP) technologies: Current status and research trends. *Renew. Sustain. Energy Rev.* **2018**, *91*, 987–1018. [CrossRef]
9. Ummadisingu, A.; Soni, M. Concentrating solar power–technology, potential and policy in India. *Renew. Sustain. Energy Rev.* **2011**, *15*, 5169–5175. [CrossRef]
10. Gharat, P.V.; Bhalekar, S.S.; Dalvi, V.H.; Panse, S.V.; Deshmukh, S.P.; Joshi, J.B. Chronological development of innovations in reflector systems of parabolic trough solar collector (PTC)—A review. *Renew. Sustain. Energy Rev.* **2021**, *145*, 111002. [CrossRef]
11. Murdock, H.E.; Gibb, D.; André, T.; Sawin, J.L.; Brown, A.; Appavou, F.; Ellis, G.; Epp, B.; Guerra, F.; Joubert, F.; et al. *Renewables 2020-Global Status Report*; REN21 Secretariat: Paris, France, 2020.
12. Yin, J.; Molini, A.; Porporato, A. Impacts of solar intermittency on future photovoltaic reliability. *Nat. Commun.* **2020**, *11*, 4781. [CrossRef]
13. Dorsey-Palmateer, R. Effects of wind power intermittency on generation and emissions. *Electr. J.* **2019**, *32*, 25–30. [CrossRef]
14. Nelson, J.A. *The Physics of Solar Cells*; Imperial College: London, UK, 2003. [CrossRef]
15. Suherman, S.; Sunarno, A.; Hasan, S.; Harahap, R. Water and heat-sink cooling system for increasing the solar cell performances. *Endorsed Trans. Energy Web* **2018**, *7*, 161050. [CrossRef]
16. Tawil, S.N.M.; Zainal, M.Z. Energy harvesting using TEG and PV cell for low power application. *Aip Conf. Proc.* **2018**, *1930*, 020041. [CrossRef]
17. Riffat, S.B.; Ma, X. Thermoelectrics: A review of present and potential applications. *Appl. Therm. Eng.* **2003**, *23*, 913–935. [CrossRef]
18. Nasu, J.; Naka, M. Spin Seebeck effect in nonmagnetic excitonic insulators. *Phys. Rev. B* **2021**, *103*, L121104. [CrossRef]
19. Singh, B.; Saoud, A.; Remeli, M.F.; Ding, L.C.; Date, A.; Akbarzadeh, A. Desing and construction of a simple thermoelectric generator heat exchanger for power generation from salinity gradient solar pond. *J. Teknol.* **2015**, *76*, 21–24. [CrossRef]
20. Singh, M.; Nirapure, S.; Mishra, A. Thermoelectric generator: A review. *J. Mech. Civ. Eng.* **2015**, *12*, 40–45.
21. Elarusi, A.H.; Fagehi, H.; Lee, H.; Attar, A. Theoretical approach to predict the performance of thermoelectric generator modules. *J. Electron. Mater.* **2016**, *46*, 872–881. [CrossRef]
22. Narducci, D. Do we really need high thermoelectric figures of merit? A critical appraisal to the power conversion efficiency of thermoelectric materials. *Appl. Phys. Lett.* **2011**, *99*, 102104. [CrossRef]
23. Bayendang, N.P.; Kahn, M.T.; Balyan, V.; Draganov, I.; Pasupathi, S. A comprehensive thermoelectric generator (TEG) modelling. In Proceedings of the Energy and Human Habitat (EHH) Conference 2020, Cape Town, South Africa, 25 November 2020. [CrossRef]

24. Snyder, G.J.; Snyder, A.H. Figure of merit ZT of a thermoelectric device defined from materials properties. *Energy Environ. Sci.* **2017**, *10*, 2280–2283. [CrossRef]
25. Mansoor, M.; Mirza, A.F.; Duan, S.; Zhu, J.; Yin, B.; Ling, Q. Maximum energy harvesting of centralized thermoelectric power generation systems with non-uniform temperature distribution based on novel equilibrium optimizer. *Energy Convers. Manag.* **2021**, *246*, 114694. [CrossRef]
26. Fernandes, A.A.; Filho, G.L.T.; Rodrigues, M.R.B. *Desenvolvimento de um Sistema Concentrador Heliotermoelétrico de Efeito Seebeck*; National Intellectual Property Institute: Brazil, 2020.
27. Rubinstein, R.Y. Optimization of computer simulation models with rare events. *Eur. J. Oper. Res.* **1997**, *99*, 89–112. [CrossRef]
28. Keith, J.; Kroese, D.P. Sequence alignment by rare event simulation. In Proceedings of the Winter Simulation Conference, San Diego, CA, USA, 8–11 December 2002; IEEE: Piscataway, NJ, USA, 2002; Volume 1, pp. 320–327.
29. Caetano, T.; Dias, W.; Lépine, J.; Monteiro, H.; Moitinho, A.; Hickel, G.; Oliveira, A. The OPD photometric survey of open clusters I. Techniques, program details and first results of robust determination of the fundamental parameters. *New Astron.* **2015**, *38*, 31–49. [CrossRef]
30. Oliveira, A.F.; Monteiro, H.; Dias, W.S.; Caetano, T.C. Fitting isochrones to open cluster photometric data. *Astron. Astrophys.* **2013**, *557*, A14. [CrossRef]
31. Zaccaro, S.J.V.; Oliveira, A.F.; Rubinger, R.M.; de Siqueira, C.C.; da Costa Junior, R.A. Determination of thickness and refractive index of SiO_2 thin films using the cross-entropy global optimization method. *Res. Soc. Dev.* **2021**, *10*, e326101019028. [CrossRef]
32. Oliveira, A.F.; Rubinger, R.M.; Monteiro, H.; Rubinger, C.P.L.; Ribeiro, G.M.; de Oliveira, A.G. Main scattering mechanisms in InAs/GaAs multi-quantum-well: A new approach by the global optimization method. *J. Mater. Sci.* **2015**, *51*, 1333–1343. [CrossRef]
33. Efron, B.; LePage, R. *Introduction to Bootstrap*; Wiley & Sons: New York, NY, USA, 1992.
34. Fernandes, A.A.; Rubinger, R.M.; Ider, J.; Oliveira, A.F.; Tiago-Filho, G.L.; Baldissera, M.R. Characterization of a solar concentration thermoelectric generator. *Eur. J. Phys.* **2021**, *42*, 065103. [CrossRef]